Available online at www.sciencedirect.com
SCIENCE DIRECT®
Journal of Power Sources 128 (2004) 278–285
JOURNAL OF POWER SOURCES
www.elsevier.com/locate/jpowsour

Aluminum-doped lithium nickel cobalt oxide electrodes for high-power lithium-ion batteries

C.H. Chen [a,b,*], J. Liu [a], M.E. Stoll [a], G. Henriksen [a], D.R. Vissers [a], K. Amine [a]

[a] *Chemical Technology Division, Argonne National Laboratory, 9700 South Cass Avenue, Argonne, IL 60439, USA*
[b] *Department of Materials Science and Engineering, University of Science and Technology of China, Anhui, Hefei 230026, China*

Received 28 July 2003; received in revised form 26 September 2003; accepted 15 October 2003

Abstract

Non-doped and aluminum-doped $LiNi_{0.8}Co_{0.2}O_2$ cathodes from three industrial developers coupled with graphite anodes were made into lithium-ion cells for high-power applications. The powder morphology of the active cathode materials was examined by a scanning electron microscope. The electrochemical performance of these cells was investigated by hybrid pulse power characterization (HPPC) testing, accelerated aging, and AC impedance measurement of symmetric cells. Although all of the fresh cells are found to meet and exceed the power requirements set by PNGV, the power capability of those cells with non-doped $LiNi_{0.8}Co_{0.2}O_2$ cathodes fades rapidly due to the rise of the cell impedance. Al-doping is found very effective to suppress the cell impedance rise by stabilizing the charge-transfer impedance on the cathode side. The stabilization mechanism may be related to the low average oxidation state of nickel ions in the cathode. The powder morphology also plays a secondary role in determining the impedance stabilization.

Keywords: Lithium nickel cobalt oxide electrode; High-power lithium-ion batteries; HPPC; Symmetric cells

1. Introduction

Because lithium is the lightest and most electronegative metal on earth, lithium batteries using metallic lithium as anode has first appeared naturally for high-energy-density applications. The evolution from lithium batteries to rechargeable lithium-ion batteries with carbon as the anode, has not changed the high-energy-density feature since carbon is also one of the lightest elements while the electrochemical potential of lithiated carbon (Li_xC) is very close to that of metallic lithium. Therefore, the most important applications of lithium-ion batteries are in the area where high-capacity or long time discharge after each charge is desired, typically in the so-called 3C (cellular phones, camcorders, and computers) industry. While R&D efforts of lithium-ion batteries continue to address the performance improvements in these fields, a lot of efforts are also under way to explore their application in other fields such as electric vehicles (EV) and hybrid electric vehicles (HEV). Unlike most of the applications, where the energy density or the capacity of the batteries is the most important concern, the EV and HEV applications require batteries with high power. The cell capacity is related to the amount of active lithium ions that are able to shuttle between the positive and negative electrodes under the operating conditions, while the power of a cell is directly related to the cell impedance or internal resistance. Obviously, these two parameters are not always associated with each other in a fresh cell; a cell of low or intermediate capacity with a small internal resistance would be considered a high-power cell. More importantly, for battery applications the capacity fade is not necessarily associated with a power fade, and vice versa. For example moisture contamination may certainly cause a capacity loss but may have a very minor effect on the cell impedance or power. Therefore, it is necessary to develop lithium-ion batteries with small and stable cell impedance.

As reported previously [1,2], Argonne National Laboratory is leading a multi-National-Lab effort in the development of suitable lithium-ion batteries for HEV applications. In our first generation baseline chemistry, we selected $LiNi_{0.8}Co_{0.2}O_2$ as positive electrode and mixed synthetic graphite as negative electrode. The lithium-ion cells made

* Corresponding author. Tel.: +86-551-360-2938; fax: +86-551-360-2940.
E-mail address: cchchen@ustc.edu.cn (C.H. Chen).

0378-7753/$ – see front matter © 2003 Elsevier B.V. All rights reserved.
doi:10.1016/j.jpowsour.2003.10.009

with this chemistry meet the power requirement set by partnership for a new generation of vehicles (PNGV). However, during the accelerated aging test at 50, 60, and 70 °C the cells lose power rather quickly. Our study with reference electrode and symmetric cell techniques has indicated that this power loss is mainly due to the cathode impedance rise, more specifically, due to the substantial increase in the charge-transfer-resistance at the interface between the cathode and liquid electrolyte [3,4]. Since the conductivity and the viscosity of the liquid electrolyte hardly change under hermetic conditions, the increase in the charge-transfer resistance is likely due to the formation of a surface layer on the cathode. Structural analyses of the Li–Ni–Co–O cathodes by several groups have confirmed the existence of this surface layer [5–9]. Therefore, to address the issue of impedance rise we take two approaches: minimize the cathode surface area and stabilize the surface reactivity of the cathode. The former approach can be realized straightforward by using cathode with reasonably large particles or different morphologies. The latter approach can be realized by using a more stable aluminum-doped cathode.

In this study, we used aluminum-doped $LiNi_{0.8}Co_{0.2}O_2$ from three industry developers as active cathode material to replace the non-doped cathode in the first generation baseline chemistry. The Al-doping level and particle morphology of the cathode material were varied in order to investigate their effects on cell performance. It will be shown that the cell impedance rise can be effectively suppressed by aluminum doping while the particle morphology plays a secondary role in this respect.

2. Experimental

2.1. Materials and laminates

The active anode material was the same as in our first generation baseline chemistry, i.e. a graphite mixture of 82 wt.% MCMB-6 and 18 wt.% SFG-6. The anode laminate was made by doctor-blade method with a slurry of 91 wt.% the graphite mixture and 9 wt.% polyvinylidene fluoride (PVDF) binder. Copper foil (20 μm thick) was used as current collector for the anode laminate. The active cathode materials of different particle morphologies were from three industry manufacturers: $LiNi_{0.8}Co_{0.2-x}Al_xO_2$ ($x = 0$ and 0.05) from manufacturer A, $LiNi_{0.8}Co_{0.2-x}Al_xO_2$ ($x = 0$, 0.05, and 0.1) from manufacturer B, and $LiNi_{0.8}Co_{0.2-x}Al_xO_2$ ($x = 0.01$, 0.02, and 0.05) from manufacturer C. These cathodes will be referred as A-LNCAO, B-LNCAO, and C-LNCAO thereafter. Cathode laminates were made also by doctor-blade method with slurries of 84 wt.% $LiNi_{0.8}Co_{0.2-x}Al_xO_2$, 8 wt.% acetylene black, and 8 wt.% PVDF. Aluminum foil (15 μm thick) was used as current collector for the cathode laminates. After calendaring, the laminate thickness is 45 μm for the anode and 60 μm for the cathode.

2.2. Fabrication of lithium-ion cells

Two types of cells were fabricated and tested in this study, i.e. 2032 coin-cells and cells with 15.5 cm^2 electrode area in a 32 cm^2 stainless steel fixture. The coin-cells were assembled in a dry room with water concentration less than 300 ppm. The 32 cm^2 cells were assembled in a glove box filled with a dry helium atmosphere. After three formation cycles at a slow rate (C/10), these cells were charged to a certain state of charge (SOC) and then disassembled in the glove box. Two symmetric cells (size 2032) were made out of each disassembled 15.5 cm^2-electrode. The electrolyte used in all of these cells was 1 M $LiPF_6$ in EC:DEC (1:1).

2.3. Hybrid pulse power characterization (HPPC) and accelerated aging tests

Hybrid pulse power characterization (HPPC) tests were conducted at room temperature with a battery cycler controlled by a VAX station for the 32 cm^2 cells after cell assembly. The test procedure was defined in the PNGV manual for high-power battery testing [10]. Accelerated aging tests were conducted with a Maccor multi-channel cycler using coin-cells. At a C/2–C/4 rate, a cell was first charged to 4.1 V and then discharged to 3 V and finally charged to 4 V at room

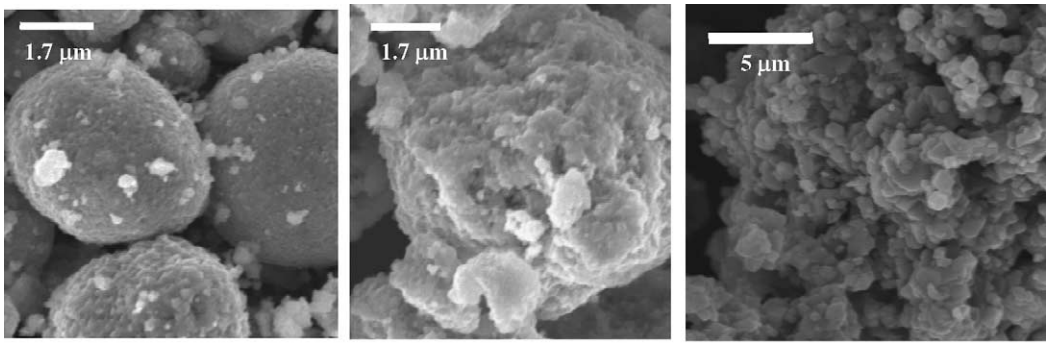

Fig. 1. Scanning electron micrographs of three cathode powders with different morphologies: A-LNCAO (a), B-LNCAO (b), and C-LNCAO (c).

temperature. During such cycling, a 30-s current interruption was performed every 10 min to derive the cell impedance at various SOC. Then the cell was aged at 50 °C in an oven for 2 days on average before the next cycling test at room temperature. By repeating the above steps, changes in the cell impedance and capacity during aging were obtained. Aging of the symmetric cells was also performed by storing the cells at 50 °C and measuring the AC impedance spectra in a short time (usually within 30 min) at room temperature every 2 days (average). The instrument was a Schlumberger model

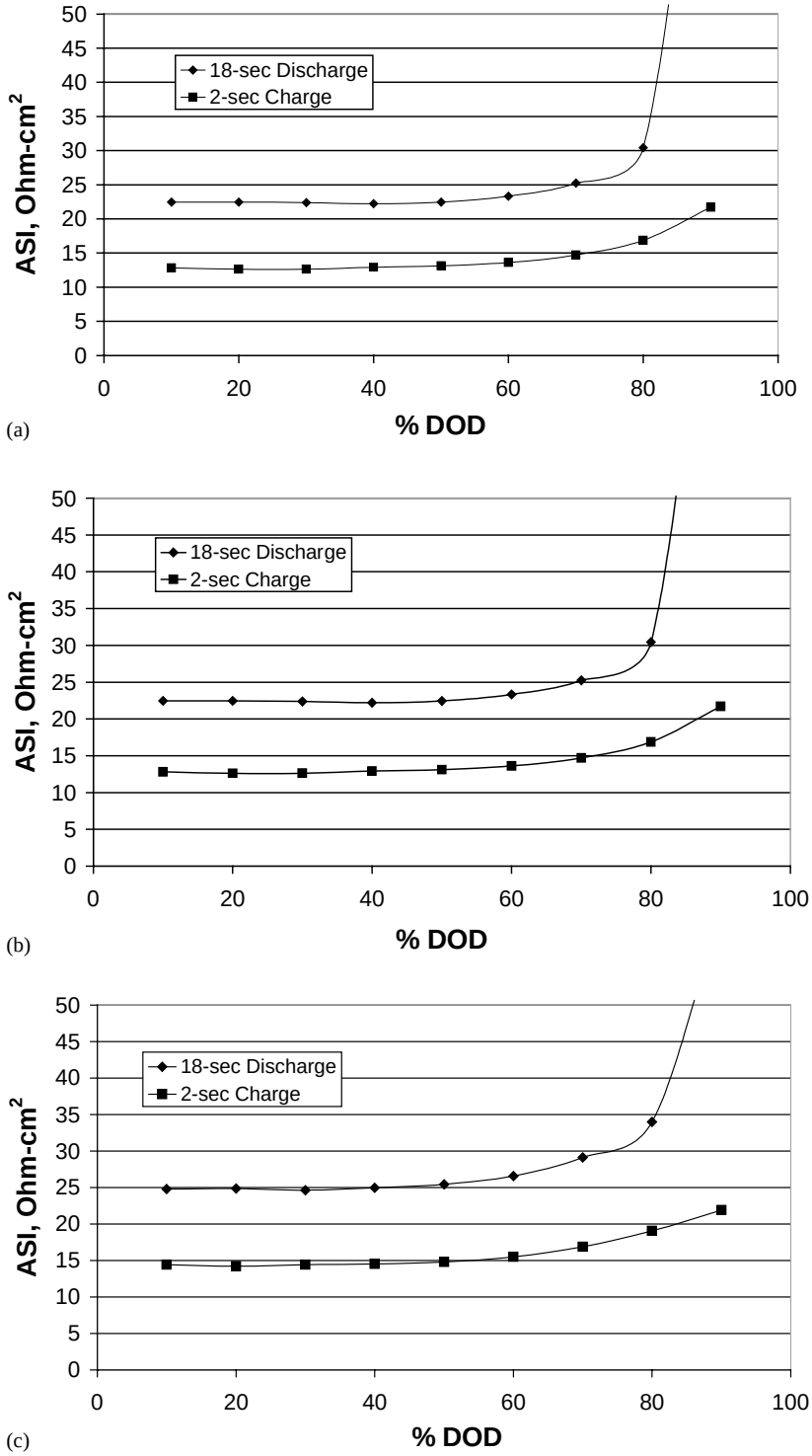

Fig. 2. Area-specific-impedance (ASI) of fresh A-$LiNi_{0.8}Co_{0.15}Al_{0.05}O_2$/graphite (a), B-$LiNi_{0.8}Co_{0.15}Al_{0.05}O_2$/graphite (b), and B-$LiNi_{0.8}Co_{0.1}Al_{0.1}O_2$/graphite (c) cells with electrolyte 1 M $LiPF_6$ in EC:DEC (1:1) at different depth-of-discharge (DOD).

1255 frequency response analyzer connected to a Schulumberger 1286 electrochemical interface and a EG&G PAR 273 potentiostat. A small (10 mV) ac perturbation and a dc bias voltage equal to the cell open-circuit-voltage (OCV) were applied with a frequency sweep from 0.01 Hz to 100 kHz during measurement.

3. Results and discussion

3.1. Powder morphology

In general, the most desirable powder morphology for lithium-ion electrodes (both cathode and anode) is relatively dense with round-edge particles, either spherical or potato-shape, in order to minimize the reactions between the electrodes and liquid electrolyte of forming surface layers and consuming cell capacity. The powder morphologies of A-LNCAO, B-LNCAO, and C-LNCAO are shown in Fig. 1. The A-LNCAO powder consists of rather dense spherical secondary particles. The average particle size is estimated to be around 3 μm from its SEM photo. The secondary particles in the B-LNCAO are also quite dense but greater in size (around 5 μm) and less spherical in shape. For the C-LNCAO powder, both the primary and secondary particles are significantly bigger than those in the A- and B-LNCAO powders. Furthermore, its secondary particles look more porous than those in the A- and B-LNCAO powders.

3.2. Initial cycling and power performance

Table 1 shows the initial capacities of the cells with Al-doped C-LNCAO. It is clear that the initial cell capacity is not affected by Al-doping as long as the Al-doping level is below 5%. Similar results are obtained for the cells with Al-doped cathodes from manufacturers A and B. However, the cell with 10% Al-doped B-LNCAO ($LiNi_{0.8}Co_{0.1}Al_{0.1}O_2$) shows a slight capacity loss (about 5 mA h/g) compared to the cathodes doped with 0–5% Al. Nevertheless, Madhvi et al. have found that more Al-doping (above 10%) can cause significant capacity loss in the case of $LiNi_{0.7}Co_{0.3}O_2$ [11].

The PNGV power requirement for the lithium-ion cells targeting hybrid electric vehicles can be translated into that the 18-s-discharge area-specific-impedance (ASI) of a cell selected to HPPC tests should be below 35 Ω cm^2 and the 2-s-charge ASI below 25 Ω cm^2 [1]. The ASI as a function of depth-of-discharge (DOD) is shown in Figs. 2 and 3 for cells with Al-doped A-, B-, and C-LNCAO cathodes. Obviously, all of the cells with Al-doped cathodes meet and exceed the PNGV requirement within large ranges of DOD. Compared to the non-doped $LiNi_{0.8}Co_{0.2}O_2$, Al-doping does not impede the power performance of the cells regardless of the powder morphology. Furthermore, comparing the effect of different Al-doping levels x from 1 to 5% (Fig. 3), it is found that 1% Al-doping results in higher ASI than 2 and 5% Al-doping. Besides, little difference is found between 5 and 10% Al-doping (Fig. 2b and c). Therefore, low

Table 1
First cycle capacities of the lithium-ion cells with Al-doped $LiNi_{0.8}Co_{0.2-x}Al_xO_2$ cathode (C-LNCAO)

x in $LiNi_{0.8}Co_{0.2-x}Al_xO_2$	Charge (mA h/g)	Discharge (mA h/g)
0.01	210	175
0.02	210	174
0.05	211	174

Cycling at 0.2 mA/cm^2 from 3 to 4.3 V.

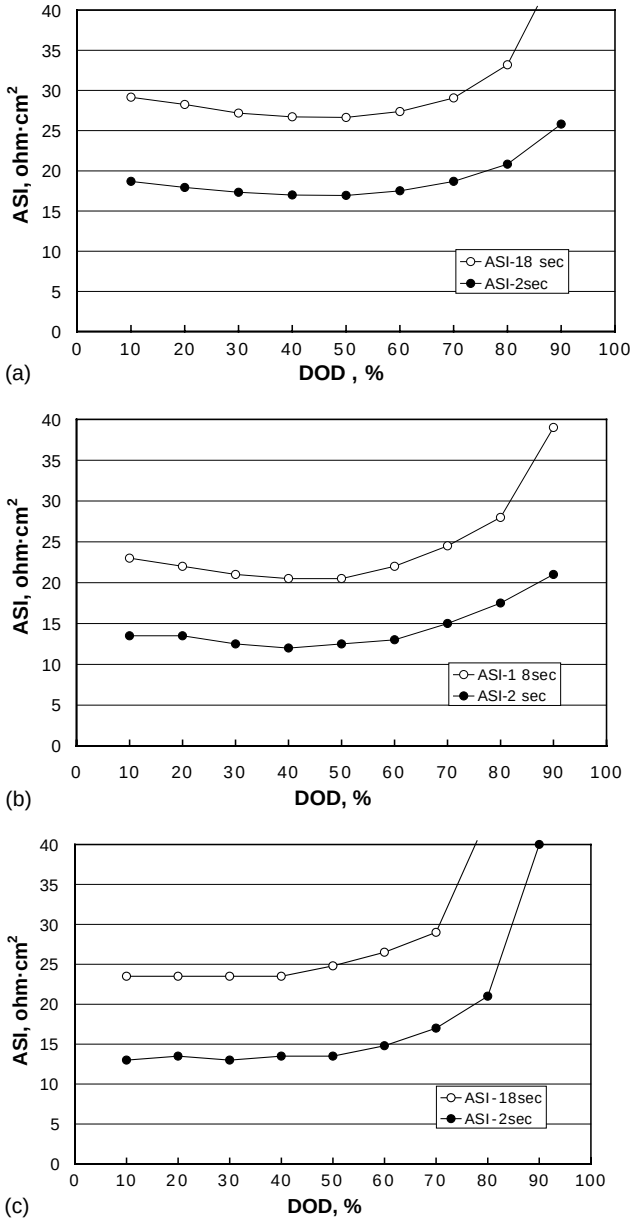

Fig. 3. Area-specific-impedance (ASI) of fresh C-$LiNi_{0.8}Co_{0.2-x}Al_xO_2$/graphite cells with electrolyte 1 M $LiPF_6$ in EC:DEC (1:1) at different depth-of-discharge (DOD): $x = 0.01$ (a), 0.02 (b) and 0.05 (c).

level (2–10%) Al-doping in $LiNi_{0.8}Co_{0.2}O_2$ can lower the impedance of a cell using these Al-doped $LiNi_{0.8}Co_{0.2}O_2$ as a cathode. This result can explain the little influence of low level Al-doping on the initial capacity. On one hand, Al is an inactive metal that is expected to lower the capacity [11]. On the other hand, the decrease of cell impedance as a result of Al-doping favors the increase of cell capacity. The trade-off of these two factors produces the unchanged capacity. Note that these HPPC measurements were conducted just after the formation cycles of these cells. As will be shown below, the impedance of some of these cells increases during aging at elevated temperatures.

3.3. Accelerated aging

For the cells with B-LNCAO and C-LNCAO, the ASI and capacity changes that occur during the accelerated aging at 50 °C are shown in Figs. 4 and 5. For the cell with 0%-Al-doped cathode (Fig. 4a), the cell ASI increases continuously from 30 to 240 Ω cm^2 during about a 1-month aging period. However, for the cells with 5 and 10% Al-doped cathodes the cell ASI remains virtually unchanged during the aging, with ASI values of approximately 30 Ω cm^2 for the former and 40 Ω cm^2 for the latter. Correspondingly, the

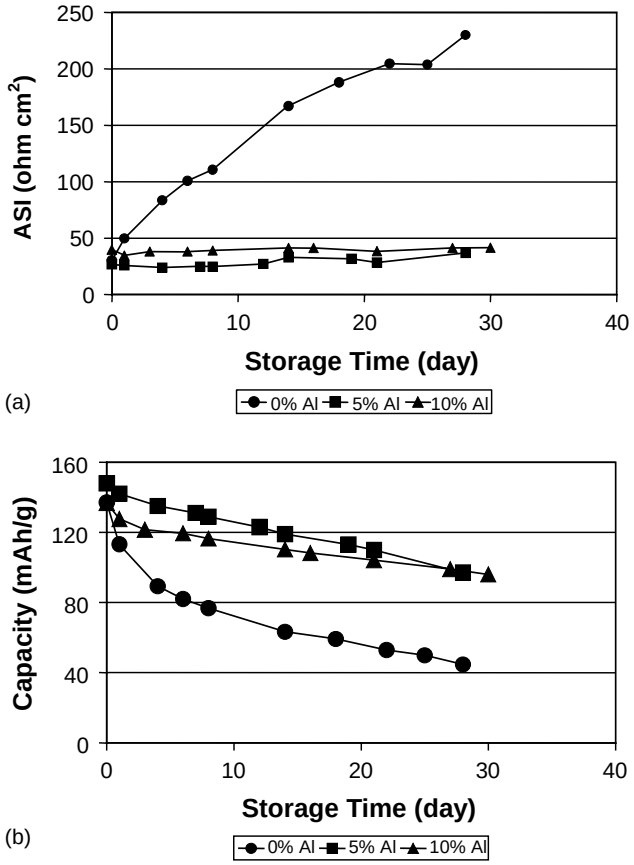

Fig. 4. Changes of ASI (a) and capacity (b) of B-$LiNi_{0.8}Co_{0.2-x}Al_xO_2$ (x = 0, 0.05, and 0.1)/graphite cells during 50 °C aging. The capacity was measured in the voltage window from 3 to 4.1 V.

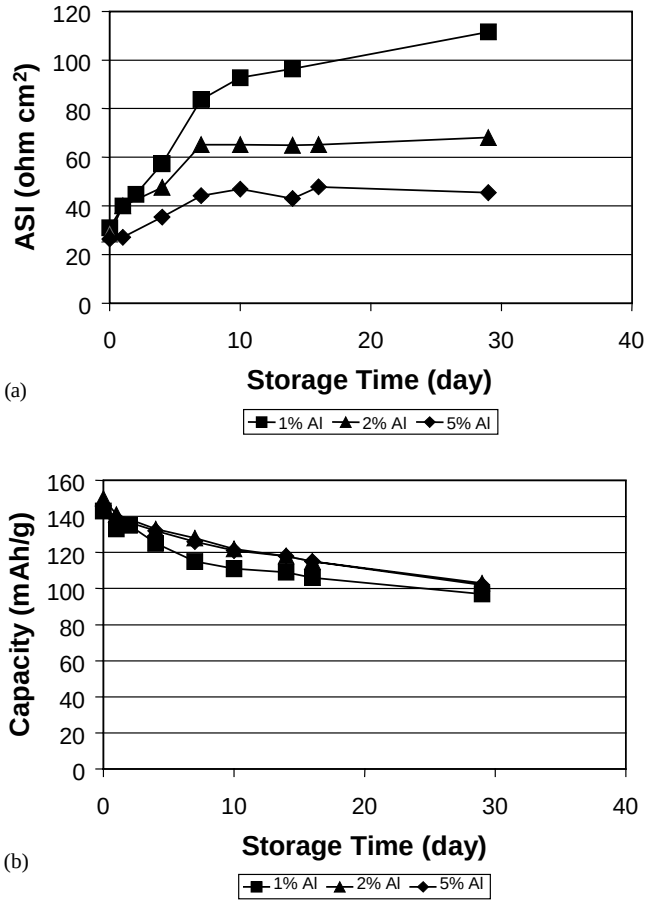

Fig. 5. Changes of ASI (a) and capacity (b) of C-$LiNi_{0.8}Co_{0.2-x}Al_xO_2$ (x = 0.01, 0.02, and 0.05)/graphite cells during 50 °C aging. The capacity was measured in the voltage window from 3 to 4.1 V.

cells with Al-doped cathodes show better capacity retention than that with the 0%-Al-doped cathode. With 1 and 2% Al-doped C-LNCAO, partial stabilization of cell impedance is observed (Fig. 5); the cell ASI increases in the first several days of aging and ceases to increase afterwards. It is noteworthy that even the cell with 5% Al-doped C-LNCAO cathode does not completely stabilize the cell impedance (Fig. 5a), which is in contrast to the cell with 5% Al-doped B-LNCAO (Fig. 4a). This difference suggests that the powder morphology may also play a secondary role in stabilizing the cell impedance. Fig. 6 shows the aging results of two cells with A- and B-type 0%-Al-doped cathodes with different morphologies. The cell with A-$LiNi_{0.8}Co_{0.2}O_2$ exhibits lower cell impedance and less impedance rise during aging than that with B-$LiNi_{0.8}Co_{0.2}O_2$. Accordingly, the capacity retention of the cell with A-$LiNi_{0.8}Co_{0.2}O_2$ is better than that with B-$LiNi_{0.8}Co_{0.2}O_2$. Again, the powder morphology shows an effect on the impedance stabilization during the accelerated aging process. By comparing the above aging results, it can be concluded that 5%-Al-doping seems the optimal percentage for both cell impedance stabilization and capacity retention.

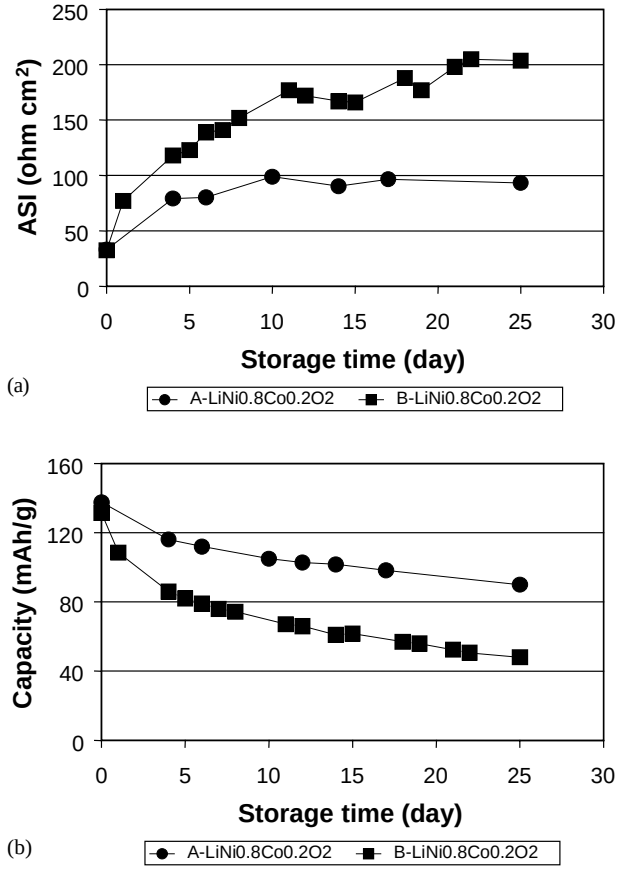

Fig. 6. Changes of ASI (a) and capacity (b) of A-$LiNi_{0.8}Co_{0.2}O_2$/graphite and B-$LiNi_{0.8}Co_{0.2}O_2$/graphite cells during 50 °C aging. The capacity was measured in the voltage window from 3 to 4.1 V.

3.4. Mechanism of impedance stabilization

Fig. 7 shows the AC impedance spectra of a symmetric anode cell (graphite/graphite) and two symmetric cathode cells (B-$LiNi_{0.8}Co_{0.2}O_2$/B-$LiNi_{0.8}Co_{0.2}O_2$, and B-$LiNi_{0.8}Co_{0.15}Al_{0.05}O_2$/B-$LiNi_{0.8}Co_{0.15}Al_{0.05}O_2$) during 50 °C aging. These symmetric cells are made from full cells charged to 4 V. Note that the impedance of the symmetric anode cell does not monotonously increase with storage time (Fig. 7a). Instead, the impedance increases in the first several days and then decreases afterwards. This phenomenon might be related to periodical buildup and dissolution of the solid–electrolyte-interface (SEI) on the graphite anode surface; yet more detailed discussion in this respect is beyond the scope of this paper. Nevertheless, it can be concluded that the graphite anode impedance does not change significantly during 50 °C aging. Therefore, the dominant contribution to any significant impedance rise of a full cell during aging should arise from the cathode side. Fig. 7b and c confirm the stabilization effect of Al-doping since a continuous and significant impedance rise is observed for the 0%-Al-doped symmetric cathode cell (Fig. 7b) while much less impedance rise is observed for the 5%

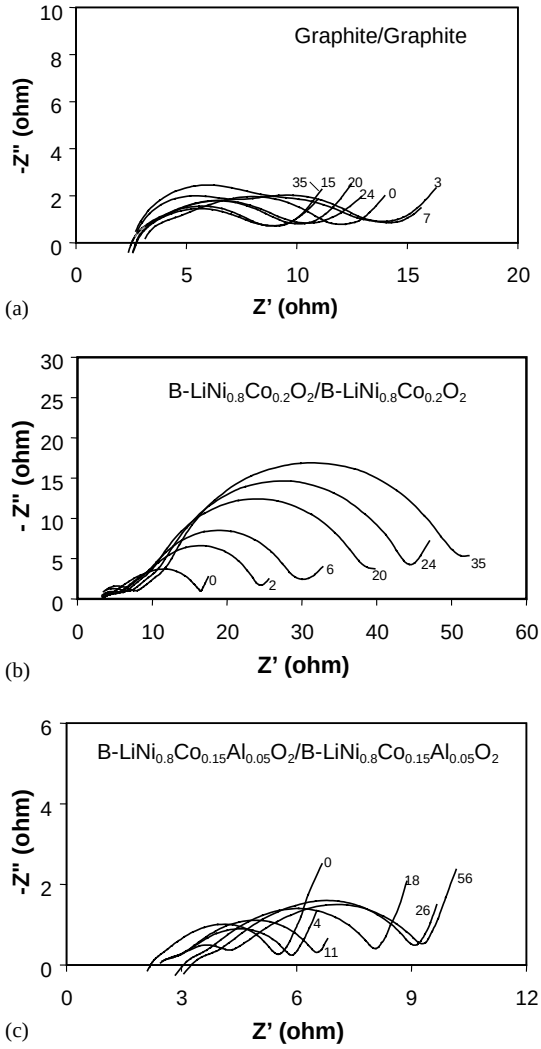

Fig. 7. AC impedance spectra of a symmetric anode cell: graphite/graphite (a), two symmetric cathode cells: B-$LiNi_{0.8}Co_{0.2}O_2$/B-$LiNi_{0.8}Co_{0.2}O_2$ (b), and B-$LiNi_{0.8}Co_{0.15}Al_{0.05}O_2$/B-$LiNi_{0.8}Co_{0.15}Al_{0.05}O_2$ (c) during 50 °C aging. The number of days in storage are indicated at the bottom of each graph.

Al-doped symmetric cathode cell (Fig. 7c). These results indicate that the cell impedance stabilization lies in the stabilization of its cathode. Notice that in Fig. 7b and c the impedance rise is mainly due to the increase of the impedance associated with the intermediate-frequency loop (approximately 0.2–40 Hz) on the impedance spectra. According to our previous studies [3,4], this loop is assigned to the charge-transfer process between the electrolyte solution and the cathode surface. Hence, the effect of Al-doping is to suppress the increase of this charge-transfer impedance. Since the electrolyte solution should not experience a marked change in its ionic conductivity and viscosity during the aging, it is reasonable to believe that there must be some continuous and marked change on the cathode surface, or the surface layer observed by other researchers [5–9].

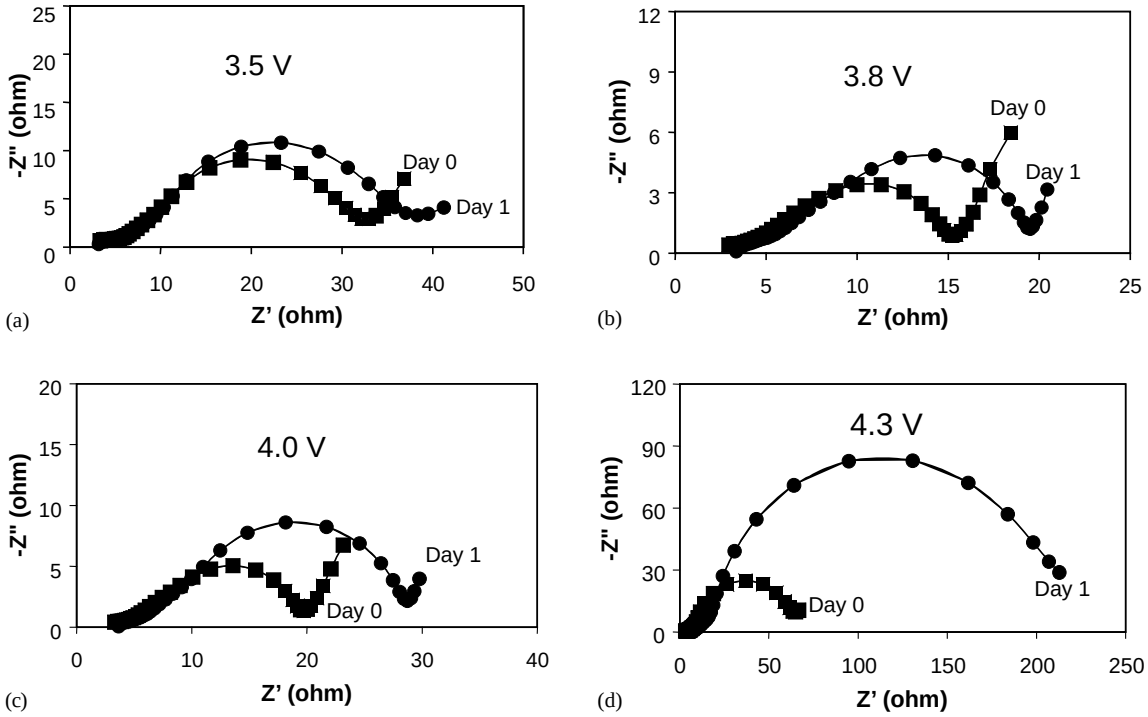

Fig. 8. AC impedance spectra of four symmetric cathode cells: B-$Li_{1-x}Ni_{0.8}Co_{0.2}O_2$/B-$Li_{1-x}Ni_{0.8}Co_{0.2}O_2$ with different states-of-charge before and after a 1-day 50 °C storage period. The cut-off voltages of the cells for making corresponding symmetric cells are indicated in each graph.

Fig. 8 shows AC impedance spectra of four symmetric cathode cells (B-$Li_{1-x}Ni_{0.8}Co_{0.2}O_2$/B-$Li_{1-x}Ni_{0.8}Co_{0.2}O_2$) with different states-of-charge before and after a day of 50 °C storage period. It can be seen that at a higher OCV, or a higher SOC, the increase of the charge-transfer impedance during the storage is substantially greater compared to the cells of lower SOC. Because a higher SOC means that the cathode contains less lithium while its nickel ions have a higher oxidation state, the impedance rise is likely associated with the oxidation of liquid electrolyte to form the surface layer on the cathode. If this surface layer is not dense, the electrolyte solution can be continuously oxidized during cycling and storage. The rate of the oxidation process is obviously related to the oxidizing ability of the cathode.

Cedar et al. have calculated the electron density of $LiAlO_2$ and Al-doped $LiCoO_2$ system [12]. They have found the electrons around oxygen ions might be able to participate in the charge–discharge process. This means that during charging or delithiation of the cathode material, the charge neutralization is maintained by partially changing the oxidation state of oxygen from −2 to −1 instead of only changing the oxidation state of the transition metal Co from +3 to +4. Assuming the same effect of Al-doping occurs in the Al-doped $LiNi_{0.8}Co_{0.2}O_2$, at the same SOC the oxidation state of nickel in the Al-doped $LiNi_{0.8}Co_{0.2}O_2$ is lower than that in non-doped $LiNi_{0.8}Co_{0.2}O_2$. Thus, the Al doping reduces the ability of oxidizing electrolyte. Therefore, the Al-doping may stabilize the charge-transfer impedance through lowering the average oxidation state of nickel ions in LNCAO system.

4. Conclusions

The lithium-ion cells with Al-doped $LiNi_{0.8}Co_{0.2-x}Al_xO_2$ ($0 \leqq x \leqq 0.1$) as cathode and graphite as anode are found promising for high-power applications. When $0 \leqq x \leqq 0.05$, the initial cell capacity is not affected by Al doping. When $x > 0.05$, the initial capacity is decreased. For the lithium-ion cells using non-doped $LiNi_{0.8}Co_{0.2}O_2$ as cathode, the cell impedance increases continuously and accordingly the power capability fades with storage time during accelerated aging at 50 °C. This impedance rise is dominantly contributed by the increase of charge transfer resistance on the cathode side. A small amount of aluminum doping in $LiNi_{0.8}Co_{0.2-x}Al_xO_2$ ($0 < x < 0.1$) cathodes significantly stabilizes the cell impedance and hence improves their power performance. In addition, the powder morphology of the active cathode material plays a secondary role to affect the stability of cell impedance: relatively dense particles are desirable.

Acknowledgements

This work was supported by the US Department of Energy, Office of Advanced Transportation Technology, under

Contract W-31-109-Eng-38. C.H. Chen also wishes to thank Academia Sinica for its support under 100 Talents program.

References

[1] K. Amine, J. Liu, ITE Lett. 1 (2000) 59.
[2] K. Amine, C.H. Chen, J. Liu, M. Hammond, A. Jansen, D. Dees, I. Bloom, D. Vissers, G. Henriksen, J. Power Sources 97–98 (2001) 684.
[3] C.H. Chen, J. Liu, K. Amine, Electrochem. Commun. 3 (2001) 44.
[4] C.H. Chen, J. Liu, K. Amine, J. Power Sources 96 (2001) 321.
[5] Y. Wang, X. Guo, S. Greenbaum, J. Liu, K. Amine, Electrochem. Solid State Lett. 4 (2001) A68.
[6] M. Balasubramanian, H.S. Lee, X. Sun, X.Q. Yang, A.R. Moodenbaugh, J. McBreen, D.A. Fischer, Z. Fu, Electrochem. Solid State Lett. 5 (2002) A22.
[7] X. Zhang, P.N. Ross, R. Kostecki, F. Kong, S. Sloop, J.B. Kerr, K. Striebel, E.J. Bairns, J. Electrochem. Soc. 148 (2001) A463.
[8] D. Ostovsky, F. Ronci, B. Scrosati, P. Jacobson, J. Power Sources 94 (2001) 183.
[9] D.P. Abraham, R.D. Twesten, M. Balasubramanian, I. Petrov, J. McBreen, K. Amine, Electrochem. Commun. 4 (2002) 620.
[10] “PNGV Battery Test Manual”, Revision 1, Idaho National Laboratory, Department of Energy, DOE/ID-10597, May 1998.
[11] S. Madhvi, G.V.S. Rao, B.V.R. Chowdari, S.F.Y. Li, J. Power Sources 93 (2001) 156.
[12] G. Ceder, Y.-M. Chiang, D.R. Sadoway, M.K. Aydinol, Y.I. Jang, B. Huang, Nature 392 (1998) 694.